

Spectroscopic study of Ceres' collisional family candidates

F. Tinaut-Ruano^{1,2}, J. de Leon^{1,2}, E. Tatsumi^{1,3}, B. Rousseau⁴, J. L. Rizos¹, and S. Marchi⁵

¹ Instituto de Astrofísica de Canarias (IAC)

Calle Vía Láctea, s/n, 38205 San Cristóbal de La Laguna, Santa Cruz de Tenerife

² University of La Laguna, Department of Astrophysics

Av. Astrofísico Francisco Sánchez, S/N, 38206 San Cristóbal de La Laguna, Santa Cruz de Tenerife

³ Department of Earth and Planetary Science, University of Tokyo, 7-3-1 Hongo, Bunkyo-ku, 113-0033 Tokyo, Japan

⁴ Istituto Nazionale di Astrofisica (INAF) - Istituto di Astrofisica e Planetologia Spaziali (IAPS)

Via Fosso del Cavaliere, 100, 00133, Rome, Italy

⁵ Southwest Research Institute 1050 Walnut St., Suite 300 Boulder, Colorado 80302 USA

Received 19/07/2021; accepted 18/11/2021

ABSTRACT

Context. Despite the observed signs of large impacts on the surface of Ceres, there is no confirmed collisional family associated with this dwarf planet. After a dynamical and photometric study, a sample of 156 asteroids were proposed as candidate members of a Ceres collisional family.

Aims. Our main objective is to study the connection between Ceres and a total of 14 observed asteroids among the candidates sample to explore their genetic relationships with Ceres.

Methods. We obtained visible spectra of these 14 asteroids using the OSIRIS spectrograph at the 10.4 m Gran Telescopio Canarias (GTC). We computed spectral slopes in two different wavelength ranges, from 0.49 to 0.80 μm and from 0.80 to 0.92 μm , to compare the values obtained with those on Ceres' surface previously computed using the Visible and Infrared Spectrometer (VIR) instrument on board the NASA Dawn spacecraft. We also calculated the spectral slopes in the same range for ground-based observations of Ceres collected from the literature.

Results. We present the visible spectra and the taxonomy of 14 observed asteroids. We found that only two of the asteroids are spectrally compatible with Ceres' surface. Further analysis of those two asteroids indicates that they are spectrally young and thus less likely to be members of the Ceres family.

Conclusions. All in all, our results indicate that most of the 14 observed asteroids are not likely to belong to a Ceres collisional family. Despite two of them being spectrally compatible with the young surface of Ceres, further evaluation is needed to confirm or reject their origin from Ceres.

Key words. asteroids – collisional family – Ceres – spectra – taxonomy

1. Introduction

Collisional families are thought to be the direct outcome of collisional events in the asteroid belt (Cellino et al. 2002). Every member in the family has similar dynamical characteristics, such as a semimajor axis, eccentricity, inclination, a longitude of perihelion, and a longitude of node, whose long-term averages are known as proper elements. Those parameters are chosen by their near constancy in collisional timing (Knezevic et al. 2002), that is to say a common collisional event with deviation by the Yarkovsky effect. However, other asteroids that do not belong to the family could accidentally acquire these orbital characteristics by a gravitational interaction with other major bodies.

Despite all the evidence of large impacts on Ceres' surface, no collisional family associated with the dwarf planet was found until a few years ago. Carruba et al. (2016) postulated the existence of this family after a dynamical study. They hypothesized that the high gravitational influence of Ceres over the outcome and the high ejection velocity that needed to escape from it should carry the family members farther from the parent body than other collisional families associated with smaller asteroids. They thus looked for candidates in the so-called

pristine region of the main asteroid belt. The "pristine region" is located between 2.825 and 2.960 au and is bordered by two main motion resonances that have remained almost empty of asteroids since its formation. There, they found a sample of 156 asteroids whose colors and visible albedo values were compatible with being fragments from Ceres, most of them having inclinations close to that of Ceres. At the end of their study, they provided a sample of 45 plausible candidates that satisfied their selection criteria. Further information can be found in Carruba et al. (2016).

In general, dynamical studies, through the use of proper elements to identify collisional families, give rise to a number of uncertainties. Discrepancies among family members are found in different authors' results (Valsecchi et al. 1989; Nesvorný et al. 2015), and cosmochemical inconsistencies in some family membership appear in different studies (Milani et al. 2014). The large photometric surveys of recent years have provided albedos at different wavelengths that give information about the composition of asteroids. This information has been combined with dynamical studies to distinguish between family members. Thus, with a few photometric points, we are able to distinguish between the main classes of asteroids. However, spectral properties in dif-

ferent wavelength ranges have been recognized as an invaluable tool in assessing the real memberships of mutually overlapping families in the space of proper elements (Knezevic et al. 2002). These spectral properties enable us to identify interlopers that are mixed within a collisional family and to get an idea of the evolution of an asteroid. In this study, our aim is to add spectroscopic information to the potential Ceres family members in Carruba et al. (2016) and check if Ceres' spectroscopic properties provide any evidence, either for or against the existence of a genetic relationship. To achieve this objective, we have observed 14 asteroids from the list of potential family members in Carruba et al. (2016) and compared these with Ceres' surface. The acquisition and reduction processes related to the ground-based data are described in Section 2. We provide details on the Ceres data in Section 3, obtained both from ground-based observations and by the Visible and Infrared Spectrometer (VIR) on board the NASA Dawn spacecraft. Data analysis is developed in Section 4, and the results obtained are presented and discussed in Section 5. Our final conclusions are expounded in Section 6.

2. Observations and data reduction

The sample of observed asteroids was selected from the dynamical study of Carruba et al. (2016), who identified a total of 156 asteroids as potential members of the Ceres collisional family, which have color photometry and/or albedos compatible with those of C-type asteroids, a diameter lower than 20 km, and a location in the pristine region. The authors mark those asteroids with a proper inclination in the range $0.098 < \sin(i) < 0.239$, which is the expected range for the Ceres family. Finally, they selected 45 asteroids that satisfied the more restrictive criteria they imposed with the aim of reducing contamination from the halo of large local families such as those of Charis, Eos, and Koronis (for further information, see Carruba et al. 2016). To simplify the notation, we label the asteroids among the more restrictive sample as subsample a, the asteroids with compatible proper inclination as subsample b, and the most general sample as subsample c. We were able to observe a total of 14 asteroids from the whole sample: five from subsample a, three from subsample b, and six asteroids from the most general subsample c.

Asteroid spectra were obtained through ground-based observations carried out with the OSIRIS instrument (Cepa et al. 2000; Cepa 2010) installed on the 10.4 m Gran Telescopio Canarias (GTC) operated by the Instituto de Astrofísica de Canarias at Roque de los Muchachos Observatory (ORM) in La Palma. Observations were executed under the "filler" (Band-C) program GTC68-17A. Filler programs are aimed to exploit telescope schedule gaps during the night that cannot be used for proposals that require better seeing and weather conditions. Observational details of the spectra obtained are shown in Table 1, including the asteroid number, date, UT starting time, exposure time, seeing and airmass values, apparent visual magnitude (m_V), phase angle (α), and distances to the Earth (Δ) and to the Sun (r) at the time of observing. Table 1 shows that seeing values varied from night to night, or even during the same night. This explains the differences in signal-to-noise ratios (S/Ns) at different asteroid spectra.

We used the R300R grism, which has a dispersion of 7.74 Å/pixel for a 0.6" slit and covers a wavelength range between 0.48 and 1 μm . A second order cutting filter is used with the grism that discards wavelengths beyond 0.92 μm . We used a 2.52" slit width to account for variable seeing conditions. The slit was oriented to the parallactic angle to minimize losses due to

atmospheric dispersion and to maximize the flux. For each asteroid, we obtained at least three spectra, offsetting the object 10" in the slit direction between individual observations. To obtain reflectance spectra of the asteroids, we observed two solar analog stars on each night at a similar airmass to that of the targets. The stars used are specified in Table 1.

The data were reduced using both IRAF¹ and a pipeline developed in Python 2.7. The data reduction steps included standard bias subtraction and flat field correction. Using the *apall* task in IRAF, we extracted 1D spectra from the 2D images, selecting an extraction aperture and a background region that changed for each target. For asteroids having low S/N (222080, 261489, and 198403), we aligned and summed the individual 2D spectra to increase the S/N before extraction. Wavelength calibration was performed using Hg-Ar, Ne, and Xe lamps. The spectra for each target were averaged, and the resulting spectrum was divided by the spectra of the two solar analogs observed each night and then normalized to unity at 0.55 μm . To obtain a reflectance spectrum of each asteroid, we averaged those two spectra obtained from two solar analogs. As a final step, we applied a phase correction to the spectra to the standard viewing geometry phase angle of 30°, following the procedure described in Ciarniello et al. (2017), who proposed the following relation between the slope in the visible and phase angle: $S_{\text{VIS}} = -9.4 \times 10^{-7} \alpha + 1.1 \times 10^{-2}$, with the angular coefficient expressed in [$\text{k}\text{\AA}^{-1} \text{deg}^{-1}$] and the intercept in [$\text{k}\text{\AA}^{-1}$], based on the observations of Ceres. The spectra obtained are shown in Fig. 1 in red. The error bars correspond to the difference between the two spectra obtained (owing to the use of two different solar analogs). For targets with a low S/N, we binned the spectra to a total of 50 points, corresponding to a binning box of about 100 Å.

3. Ceres data

To compare our visible spectra with the spectra for Ceres, we searched the literature for any spectral data already published from ground-based and space-based data. We compiled different ground-based visible spectra of Ceres from previous studies: one in the S³OS² survey (Lazzaro et al. 2004), with a phase angle of 16°; one in the SMASSII survey (Bus & Binzel 2002b), with a phase angle of 18.5°; and another obtained by Vilas & McFadden (1992) at a phase angle of 6.1°. We also included the six spectrophotometric observations from the Eight color Asteroid Survey (ECAS) (Zellner et al. 1985) obtained with phase angles between 8° and 22°. We excluded the spectra from the 24 color Asteroid Survey (Chapman & Gaffey 1979; McFadden et al. 1984) because of their high noise at the longer wavelengths of the visible range. We also applied a phase correction to the ground-based data for Ceres, using the same procedure as in Ciarniello et al. (2017). All these spectra have a wavelength range comparable to or greater than that of our spectra obtained with the OSIRIS instrument. For the ECAS data, we computed the reflectance values at OSIRIS wavelength limits (0.49 and 0.92 μm) by interpolating the nearest filters. The area covered by the different spectra is represented by a gray hatch in the upper left panel of Figure 1. We computed the mean of all the ground-based spectra in the same wavelength range as that of our observations and used this ground-based mean spectrum to compute the spectral slopes. Again, the errors are given by the variations between the different spectra.

¹ Image Reduction and Analysis Facility: <http://iraf.noao.edu>

Asteroid	Date	UT	T _{exp} (s)	seeing (")	airmass	m _V	α (°)	Δ (au)	r (au)	Solar analogs	sample
61674	12/04/2017	22:16	3x300	1.4	1.15	18.1	15.5	1.74	2.56	1,3	a
66648	10/04/2017	01:16	3x600	1.8	1.13	19.8	6.0	2.32	2.28	2,1	a
20094	10/04/2017	05:14	3x600	1.8	1.20	19.7	14.4	2.50	3.21	2,1	a
222080	10/04/2017	03:02	9x300	1.7	1.20	20.1	3.4	2.30	2.29	2,1	a
	17/04/2017	02:17	3x900	0.8	1.20	20.1	3.2	2.29	3.28	2,1	a
261489	17/04/2017	01:06	3x900	0.8	1.40	21.1	15.3	2.63	3.27	2,1	a
5994	10/04/2017	00:15	3x300	1.8	1.20	18.0	15.0	2.95	3.50	2,1	b
23000	10/04/2017	02:00	3x300	2.3	1.07	18.1	7.6	2.02	2.97	2,1	b
198403	10/04/2017	04:16	3x300	1.8	1.24	20.3	20.5	2.25	3.18	2,1	b
		04:32	4x450	1.8	1.30						
6671	12/04/2017	21:23	3x300	1.5	1.14	18.5	18.0	2.86	3.19	1,3	c
22540	12/04/2017	21:51	3x300	1.4	1.05	19.1	19.1	2.21	2.78	1,3	c
20095	17/04/2017	02:52	3x300	1.1	1.50	19.0	5.0	2.08	3.06	2,1	c
121281	17/04/2017	01:25	3x600	1.1	1.40	19.6	6.2	2.01	2.98	2,1	c
38466	17/04/2017	03:21	3x300	1.4	1.60	19.0	10.5	1.90	2.81	2,1	c
155547	17/04/2017	02:07	3x600	1.1	1.30	19.9	1.7	2.25	3.25	2,1	c

Table 1. Observational details of the observed asteroids. The solar analog stars used are 1:SA102-1081, 2:SA107-998, and 3:SAM67-1194. The last column refers to the subsamples identified in this work from the general list of potential Ceres family members in Carruba et al. (2016).

Regarding the space-based data, the NASA Dawn spacecraft visited Ceres in 2015. From the first observations, we know that there is spectral variation on its surface (Nathues et al. 2016). Reddy et al. (2015) found variations in the band depth near 1.1 μm that are to be correlated with albedo, and in the spectral slope related to the phase angle and longitude. If our observed asteroids did indeed originate from a collision with Ceres in the past, they would show a spectral variation similar to that observed on the surface of the dwarf planet. In order to compare the asteroid spectra with the observed spectral variation on the surface of Ceres. We used the spectral slope data calculated by Rousseau et al. (2020) with the visible channel of the VIR spectrometer (de Sanctis et al. 2011). VIR is a mapping spectrometer with a moderate spectral resolution (0.002 μm in the visible range) and it covers a wider wavelength range than OSIRIS (from 0.25 μm to 1.0 μm). The mapping capability of VIR allowed us to provide almost complete coverage of the surface of Ceres during the Dawn mission.

Rousseau et al. (2020) produced spectral parameter maps of the surface of Ceres for latitudes from 60°S to 75°N. They calculated the spectral slope for the whole surface in three wavelength ranges: the visible to near-ultraviolet (S_{VNUV} , 0.405-0.465 μm), the visible (S_{VIS} , 0.480-0.800 μm), and the visible to near-infrared (S_{VNIR} , 0.800-0.950 μm). They also calculated the albedo at 0.550 μm and several color ratios. In this study we used those spectral maps only at medium latitudes (from -60° to 60°) to avoid high phase angles, shadows, and bright regions that might otherwise be introduced by high incidence and emission angles. In order to adapt the map's spatial resolution to the size of our sample asteroid (~ 10 km), we binned it in $1^\circ \times 1^\circ$ bins, ~ 100 km² at medium latitudes of the surface of Ceres.

4. Data analysis

After obtaining the final reflectance spectra for each ground-based observed asteroid, we classified them using the so-called Bus taxonomy (Bus & Binzel 2002a), which is one of the most comprehensive taxonomies based on a total of 1447 visible spectra of asteroids. We carried out a visual classification following the criteria described in Bus & Binzel (2002a), which include

the following: the existence of local maximum, a wavelength at which the slope changes, how much slope changes before and after the maximum (if it exists), and a visible slope value. We also used a computational classification taking advantage of the online tool M4AST.² (Popescu et al. 2012) This tool fits a curve to the data and compares it with taxonomic classes defined by DeMeo et al. (2009), which is an extension to the near-infrared of the Bus taxonomy, using χ^2 to evaluate this comparison. In terms of the Bus taxonomy, Ceres belongs to the primitive C complex, which is characterized by a flat, featureless spectra.

An absorption band at 0.7 μm is usually found in primitive asteroids. The band is associated with Fe bearing hydrated minerals, such as phyllosilicates (Vilas & Gaffey 1989), implying the presence of liquid water at some instances in the the lifetime of the asteroid (Vilas 1994; Fornasier et al. 1999; Rivkin 2012; Fornasier et al. 2014). This band is also interesting because it is related to the band observed at 3 μm , which is also associated with hydrated silicates and present in Ceres (Vilas 1994). When the 0.7 μm is present, we usually observe the 3 μm band. However, the converse is not true; that is to say, the absence of an absorption band at 0.7 μm does not imply the absence of hydrated silicates (Vilas 1994). When the 0.7 μm band was found to be present in our asteroid spectra, we studied it by subtracting the continuum (a line connecting the two reflectance maxima in the wings of the band) and fitting a Gaussian function. From this fit we obtained the central wavelength (the minimum of the Gaussian) and the depth of the band (as a percentage). The error in these parameters is given by the differences between the resulting spectra when dividing the solar analogs.

To know how different an asteroid could be from Ceres, we first studied the distribution of the spectral slope for the surface of Ceres. To do this, we used the global maps with calculated spectral slopes in Rousseau et al. (2020) and computed the spectral slopes in our target asteroids using the same definition as in Rousseau et al. (2020) and adopted from Ciarniello et al. 2015,

² <http://spectre.imcce.fr/m4ast/index.php/index/home>

2017. The spectral slope in a wavelength range (λ_1, λ_2) is given by

$$S_{(\lambda_1, \lambda_2)} = \frac{\left(\frac{I}{F}\right)_{\lambda_2} - \left(\frac{I}{F}\right)_{\lambda_1}}{\left(\frac{I}{F}\right)_{\lambda_1} \times (\lambda_2 - \lambda_1)}, \quad (1)$$

where $(I/F)_{\lambda_1}$ is the calibrated radiance factor or reflectance measured at λ_1 . With this definition, Rousseau et al. (2020) computed three different slopes, S_{VNUV} , S_{VIS} , and S_{VNIR} , as described in Section 3. The instrumental setup used with OSIRIS at the GTC provides an effective wavelength range between 0.49 and 0.92 μm ; we thus computed the asteroid's visible spectral slope between 0.49 and 0.80 μm and the visible near-infrared slope between 0.80 and 0.92 μm . As those spectral regions are mainly flat and linear in C complex asteroids, except for the 0.7 μm band (if present), the difference when using a slightly shorter wavelength range is not significant.

5. Results and discussion

5.1. Comparison between the sample and Ceres

The visible spectra of the observed asteroids are shown in Figure 1. The variation in ground-based spectra of Ceres used in this study is shown as a gray hatched area. This variation can be explained by several observational issues, such as bad slit centring, solar analog discrepancies, and differences in airmass between the asteroid and the solar analogs. As the spectra were collected from the literature, we do not have access to such information, with the exception of the phase angles, for which we already applied a correction following Ciarniello et al. (2017).

We observed a variety of asteroid classes in our sample. As Ceres is a carbonaceous asteroid, one would expect the asteroids of its family to also be carbonaceous. Taxonomic classes with a carbonaceous composition belong to the C complex, and X types with a low albedo (mainly Xc types). Other primitive taxonomic classes such as end member T and D types have steep, red slopes associated with the presence of processed organics typical of outer belt asteroids, Trojans, and cometary nuclei which are supposed to form in the cold outer solar system (Fujiya et al. 2019) and, therefore, to be less compatible with an origin in a C-type asteroid as Ceres. We show the taxonomic classification and computed slopes in Table 2. The results of our visual classification (following the procedure described in Section 4) are listed in the second column of the table, while the third and fourth columns show the best two fits (with their associated χ^2 value) obtained with the M4AST tool. As can be seen in the table, there are some discrepancies in the results between the visual and the computational classifications in terms of the specific taxonomic classes, but the agreement is generally quite good. Considering these results, we assigned the asteroids to one of the three major taxonomic complexes (the C, X, or S complex), as can be seen in the fifth column of the table.

Regarding the major discrepancies found, the M4AST tool classifies asteroid 22540 as a C-type object. However, the observed maximum at 0.75 μm and the drop in reflectance upwards of 1 μm suggest an S-type classification after visual inspection of its spectrum, which is even flatter than usual S-type asteroids. In the case of the three asteroids having low S/N (222080, 198403, and 261489), we used the general behavior of their spectra to classify them. Asteroid 222080 has a flat and featureless spectrum that could belong to spectral types C or X, but the high VNIR spectral slope made us include it in the X complex. The

high spectral slope of asteroid 198403 suggests that it is a D-type asteroid. The dispersion in the data points of the 261489 spectrum makes it almost impossible to provide a reliable classification. The variety of taxonomic complexes and classes that we have found in our sample of 14 asteroids (C, X, S, and D) indicates that not all of them belong to the same collisional family. Four out of 14 of our observed asteroids belong to the C complex: 61674 from subsample a; 5994 and 23000 both have an inclination in the same range as Ceres; and 6671 from subsample c (the initial sample in Carruba et al. 2016). We found another four asteroids in the X complex: 20094 and 222080, from subsample a, and 121281 and 155547 from subsample c.

To go further, we analyzed the slope distribution on the surface of Ceres, using the spectral data provided by Rousseau et al. (2020) and described in Section 3. The distribution of slopes on the surface of Ceres, binned in $1^\circ \times 1^\circ$ areas, is shown in the $(S_{\text{VIS}}, S_{\text{VNIR}})$ density plot of Figure 2. Where we have superimposed the slopes (and their errors) computed for the asteroids belonging to the C complex as green boxes, those belonging to the X complex as blue boxes, and those belonging to the S complex as light brown boxes. It is interesting to note here that those asteroids in the C complex are actually those located closer to the populated region in this density plot. Figure 3 is a zoom into this densest region; we have also plotted in dark gray the computed slopes for the average ground-based spectrum of Ceres (see Table 2). The distribution shows that the median slope values (blue cross in Fig. 3) are $S_{\text{VIS}} = 2.49 \times 10^{-5} \text{ \AA}^{-1}$ and $S_{\text{VNIR}} = -1.94 \times 10^{-5} \text{ \AA}^{-1}$. We notice an asymmetry in the distribution in the bottom left side from the median point, where there seems to exist an over dense direction. This is studied in Section 5.3.

As we can see in Fig. 3, there is a difference between the slopes computed from ground-based spectra of Ceres (dark gray box) and the values obtained from spacecraft data. According to Carrozzo et al. (2016), Dawn/VIR spectra are affected by a positive slope in the VIS to NIR range when compared to ground-based spectra of the same target, an effect for which the origin is not currently understood. In addition, several effects (see first paragraph of Section 5.1) can affect the spectral slopes when measured from the ground. Thus, with the aim of avoiding all of these discrepancies, we only compared the slope distributions in a relative way: asteroids from the ground relative to Ceres from the ground and slopes in the surface of Ceres relative to their median value. To visualize the results more clearly, we provide the results of Fig. 3 in Fig. 4 in this relative way. The black, blue, and green contours correspond to the 99.7%, 95%, and 68% most usual values, that is the 3σ , 2σ , and 1σ distance to the median, respectively. In other words, if the distance from the asteroid spectral slopes to the center of the distribution in this new figure exceeds the 1, 2, or 3σ contours, it means that the slope values of the asteroid are further from those of Ceres than 68%, 95%, or 99.7% of the slope values of the surface of Ceres to the median value. Thus the asteroid is less likely to be constituted of the same material as the surface of Ceres. Based on this analysis, we may conclude that, taking the errors into account, the slopes of 6671 lies inside the 1σ contour and the slopes of 61674 have a difference with the slopes of Ceres smaller than the 2σ contour. Furthermore, 6671 has an absorption band at 0.7 μm that we study further in the next section. Another hint is that asteroid 61674, which belongs to the preferred samples of Carruba et al. (2016), lies near the overdense direction observed in the histogram and mentioned earlier in this section. Asteroids 5994 and 23000 are further from the 3σ contour, meaning that its slope values differ by more than the 997% variation of the

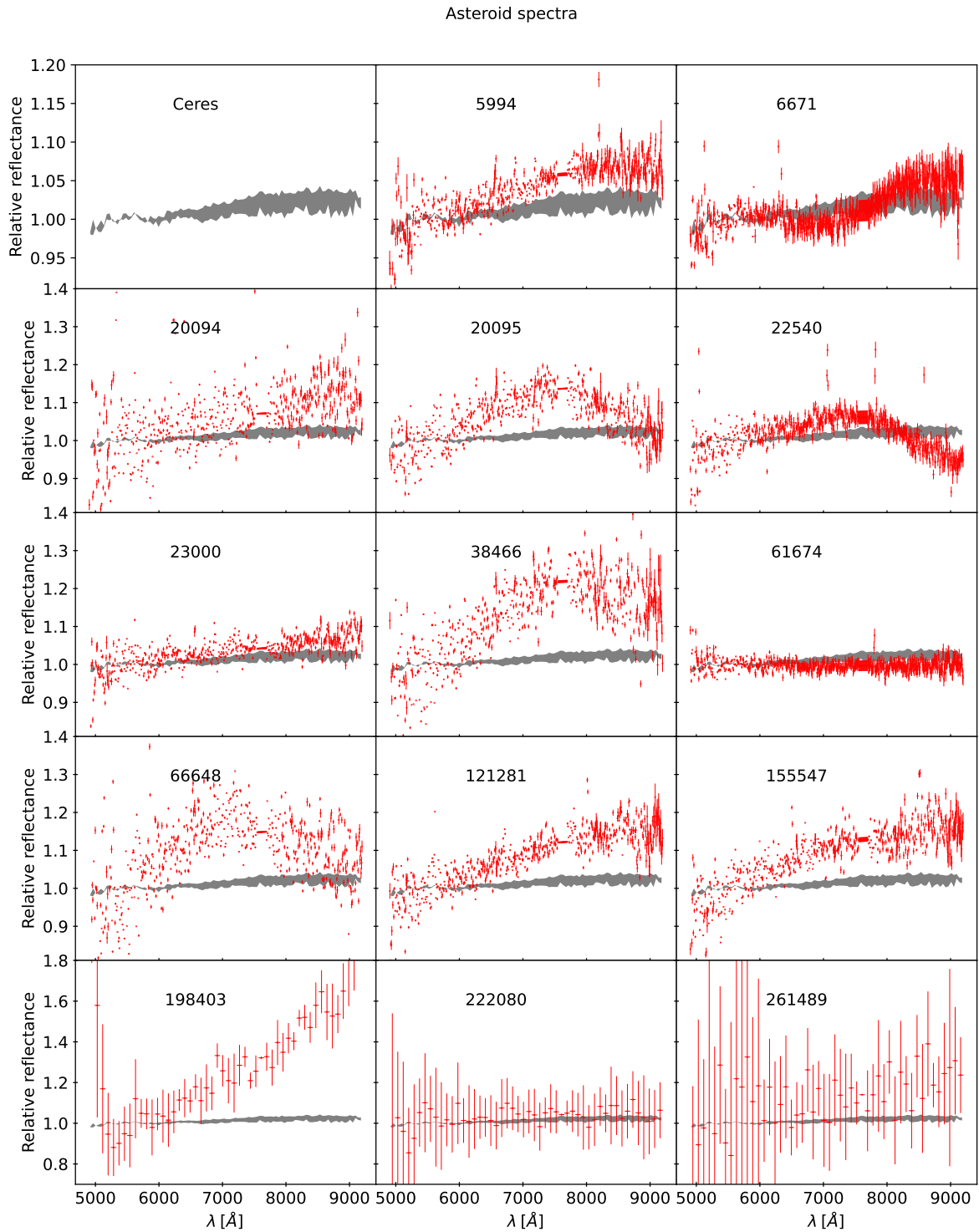


Fig. 1. Visible reflectance spectra of the observed asteroids (in red), normalized to unity at $0.55 \mu\text{m}$ and phase corrected. The upper left panel shows the area covered by the different ground-based spectra of Ceres used in this study (see Section 3 for details). This variation is superposed on the spectra of each asteroid in the other panels as a gray hatched area. For asteroids with a low S/N, we applied a binning factor of ~ 10 , obtaining 50 point spectra.

Asteroid	Visual	M4AST - χ^2 (10^{-3})		Complex	S_{VIS} (10^{-5}\AA^{-1})	S_{VNIR} (10^{-5}\AA^{-1})	Sample
61674	B	Ch - 0.182	B - 0.342	C	-1.7 ± 0.6	-0.2 ± 0.6	a
6671	Ch	Cb - 0.191	Cgh - 0.274	C	1.4 ± 0.7	1.6 ± 0.5	c
5994	C	Cgh - 0.192	C - 0.235	C	4.4 ± 0.3	-1.0 ± 0.7	b
23000	C/Cb	Cgh - 0.077	C - 0.138	C	3.4 ± 0.8	1.6 ± 0.6	b
20094	X	Xc - 0.169	X - 0.224	X	7.9 ± 2.0	0.9 ± 0.7	a
121281	X	X - 0.242	Xc - 0.253	X	5.6 ± 0.8	0.9 ± 2.2	c
155547	Xk	Xe - 0.100	Xk - 0.455	X	7.3 ± 1.0	1.3 ± 2.2	c
222080	C/X?	O - 15.773	V - 17.429	X	2 ± 4	6.3 ± 1.3	a
198403	D?	Cb - 31.374	X - 32.408	D	16.0 ± 0.3	40.3 ± 1.3	b
66648	S	Sq - 0.448	Sr - 0.609	S	13 ± 6	-4.2 ± 1.4	a
20095	Sq	Sq - 0.458	Sr - 0.654	S	5.4 ± 0.8	-9.0 ± 2.0	c
38466	S	S - 0.353	Sv - 0.393	S	8.2 ± 0.8	-7.0 ± 2.0	c
22540	Sq	B - 0.916	Cg - 1.166	S	3.7 ± 0.9	-8.3 ± 0.5	c
261489	-	A - 21.854	L - 26.925	-	1 ± 4	8 ± 4	a
Ceres	C	C - 0.0096	Cb - 0.1087	C	1.2 ± 0.5	0.2 ± 0.9	

Table 2. Taxonomic classification (both visual and using the M4AST online tool), as well as the computed spectral slopes for the observed asteroids. The last column shows the sample to which asteroids belong (see main text for details).

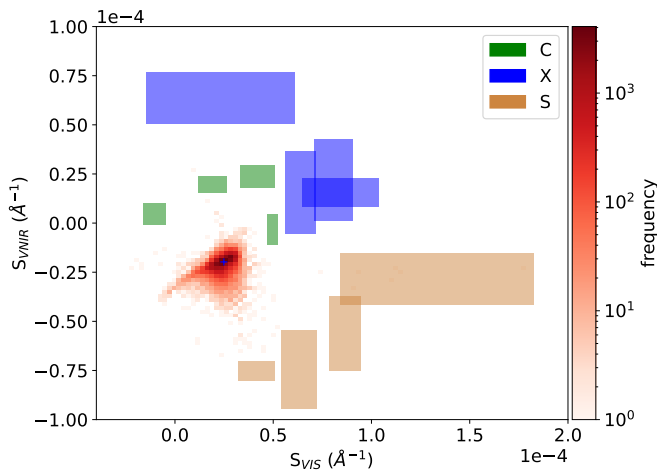


Fig. 2. 2D density distribution of spectral slopes S_{VIS} and S_{VNIR} in the surface of Ceres, computed from the Dawn/VIR data, provided by Rousseau et al. (2020) and binned in $1^\circ \times 1^\circ$ boxes. Computed slopes (and their errors) for the targeted asteroids belonging to the C complex (green boxes), X complex (blue boxes), and S complex (yellow boxes). The median slope values of the surface of Ceres are represented by a blue cross.

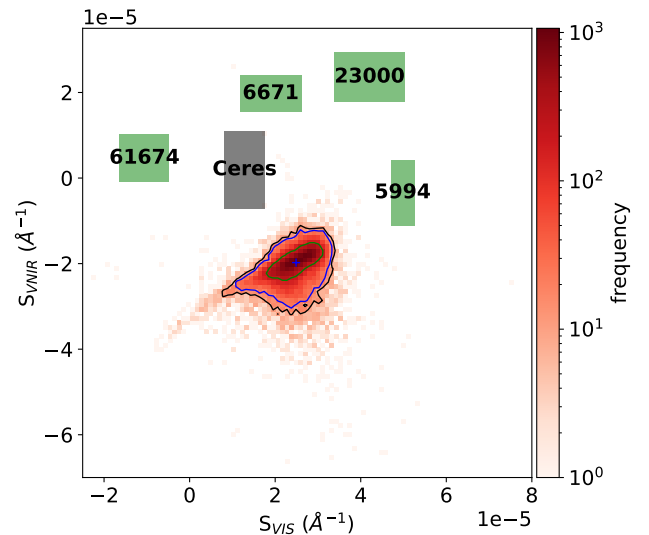


Fig. 3. Same as Fig. 2, but with a zoom into the densest region. Computed slopes (and their errors) for both the targeted C complex asteroids and ground-based average spectrum of Ceres are overplotted with green and dark gray boxes, respectively. The median slope value of the surface of Ceres are represented by a blue cross. The black, blue, and green contours correspond to the 99.7%, 95%, and 68% most usual values, i.e., 3σ , 2σ , and 1σ distance to the median.

surface of Ceres. That leaves two out of the 14 initial asteroids as candidates to be spectrally similar candidates to Ceres.

5.2. Asteroid 6671: A $0.7\mu\text{m}$ absorption band

As we can see in Fig. 1, asteroid 6671 has an absorption band around $0.7\mu\text{m}$. The two individual spectra of 6671 obtained using two different solar analogs are shown in Fig. 5 after continuum removal (following the procedure described in Section 4), together with the Gaussian fit and the corresponding derived parameters (wavelength position of the center of the band and band depth, as percentages).

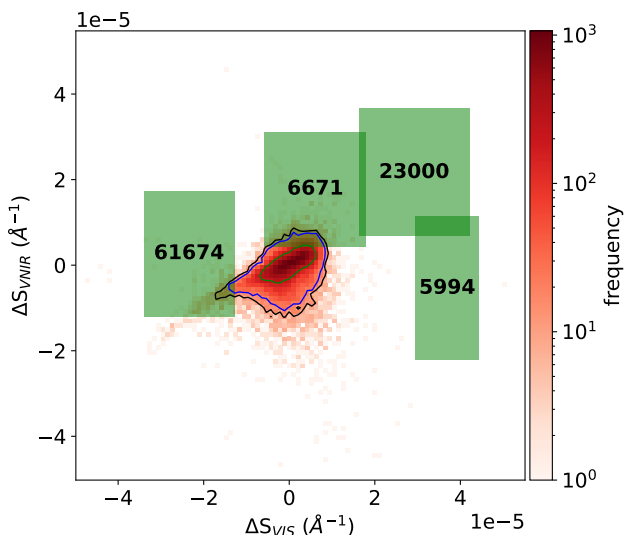


Fig. 4. Same as Fig. 3, but for the differences in S_{VIS} and S_{VNIR} between the C-type asteroids and ground-based spectrum of Ceres. The distribution of slopes on the surface of Ceres, as measured by Dawn/VIR, is relative to the median value.

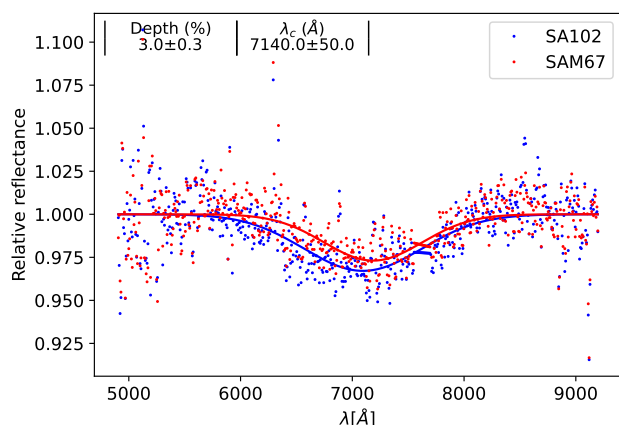


Fig. 5. Individual spectra of asteroid 6671 obtained using two solar analogs (Landolt SA102-1333 - SA102, and SAM67-1194 - SAM67) and with the continuum removed. Gaussian fits to the band for both spectra are represented with continuous lines. The average band depth (%) and wavelength position of the center of the band (λ_c) are also shown.

The detection of a $0.7 \mu\text{m}$ in ground-based spectra of Ceres has only been reported by Perna et al. (2015) with an absorption depth smaller than 0.7%. On the contrary, absorption bands in the $3 \mu\text{m}$ region are clearly detected, both in ground-based and space data, and they are associated with the presence of phyllosilicates, iron-rich clays, and carbonates (Lebofsky et al. 1981; Vernazza et al. 2005; Rivkin et al. 2006; de Sanctis et al. 2015; Usui et al. 2019). In addition, a subtle absorption band at $0.6 \mu\text{m}$ was reported in Ceres by Vilas et al. (1993) and later confirmed by Fornasier et al. (1999), which was produced by charge transfer in aqueous alteration products. Interestingly, Rizos et al. (2019) identified an absorption band at $0.7 \mu\text{m}$ around the Occator crater of Ceres using data from the Dawn Framing Camera, and they measured the band depth and the wavelength position of its center: depth = $3.4 \pm 1.0\%$ and $\lambda_c = 6980 \pm 70 \text{ \AA}$. Our

results for asteroid 6671 (depth = $3.0 \pm 0.3\%$ and $\lambda_c = 7140 \pm 50 \text{ \AA}$) are in good agreement with those obtained by Rizos et al. (2019). It is important to note here, however, that these similarities are not unique or exceptional: the values obtained for the $0.7 \mu\text{m}$ absorption band in 6671 are also in agreement with typical values found in other primitive asteroids throughout the main belt ($2.8 \pm 1.2\%$ and $6914 \pm 148 \text{ \AA}$, Fornasier et al. 2014) and in the primitive collisional families of the inner belt ($2.8 \pm 1.3\%$ and $7065 \pm 160 \text{ \AA}$ for Erigone in Morate et al. 2016; $2.2 \pm 0.6\%$ and $7000 \pm 150 \text{ \AA}$ for Klio, $3.1 \pm 0.8\%$ and $7110 \pm 130 \text{ \AA}$ for Chaldaea, and $2.9 \pm 1.2\%$ and $7100 \pm 150 \text{ \AA}$ for Chimaera in Morate et al. 2018).

Furthermore, the collision that generated the Occator crater (about $17.8 \pm 1.2 \text{ Ma}$ ago, Stephan et al. 2019, more recently dated by Neesemann et al. (2019), who obtained an age of $21.9 \pm 0.7 \text{ Ma}$) could not be the progenitor of a collisional family, as the diameter of this crater is 92 km and according to Carruba et al. (2016) the expected size of the progenitor is over 200 km. Thus, the presence of this band is not a reason to infer an origin of asteroid 6671 from Ceres.

5.3. Asteroid 61674: The overdensity region in spectral slope density plot

We noticed that asteroid 61674 lays in a particular place of the density plot shown in Fig. 4, near the asymmetric dense region observed in the bottom left side of the plot. This region is mainly correlated with cratered surface of Ceres.

To study the nature of this behavior, we measured the spectral slopes of 26 different craters with measured diameters and ages based on the crater chronology collected by Stephan et al. (2019); more information about them is given in Table 3. In order to compare these slopes with those measured in regions outside the craters, we used a larger sample of craters from Hiesinger et al. (2016): we first selected the region inside each crater on our cylindrical projection map; we then modeled the craters as an ellipse with the semimajor axis (a) as the given radius in degrees and semiminor axis $b = a \times \cos(\phi)$, with ϕ being the latitude; finally, once all of the cratered regions were identified, we used this information to mask the map and to extract the data from noncratered surface. In Fig. 6 we show the median slope for each dated crater (Stephan et al. 2019) over the density plot, clearly following the overdensity region. In Fig. 7, we present the median value for each dated crater versus age and diameter in the three wavelength ranges defined by Rousseau et al. (2020) (see Section 3). The ages were obtained using two different models: the asteroid derived model (ADM) (Marchi et al. 2012, 2016) and the lunar derived model (LDM) (Hiesinger et al. 2016), as explained in Stephan et al. (2019). Both models are based on crater size-frequency distribution measurements: the LDM uses direct crater observations at the surface of the Moon, and the ADM uses observations of objects in the main asteroid belt (Hiesinger et al. 2016). However, both have limitations: the LDM assumes that the flux of the impacting projectiles in the asteroid belt had the same variations in the size frequency and flux of impacts as there were in the Moon, which is inconsistent with current observations; on the other hand, ADM uses only observable asteroids, bigger than $\sim 3 \text{ km}$ radius which generate $\sim 20 \text{ km}$ diameter craters. For smaller craters an extrapolation of the model is needed (Hiesinger et al. 2016). We include in Fig. 7 the median slope values for the

surface outside every crater in [Hiesinger et al. \(2016\)](#).

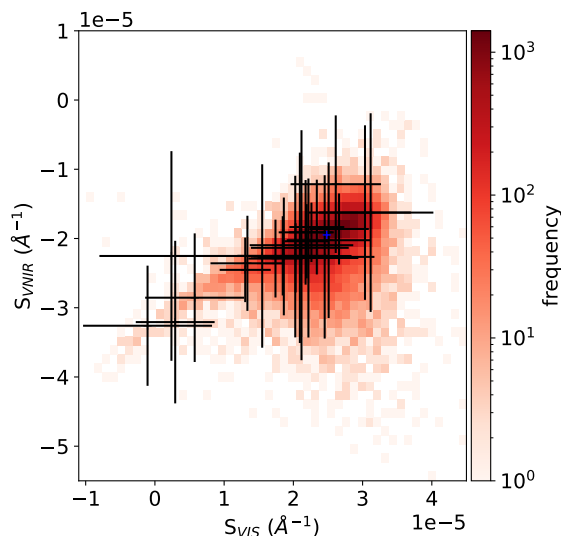


Fig. 6. 2D density distribution of spectral slopes S_{VIS} and S_{VNIR} on the surface of Ceres, computed from the Dawn/VIR data, provided by [Rousseau et al. \(2020\)](#) and binned in $1^\circ \times 1^\circ$ boxes. The median slope value for each crater from [Stephan et al. \(2019\)](#) and its standard deviation is represented with a black cross.

In the visible range, we found a Pearson correlation coefficient between the spectral slope and $\ln(t)$ of 0.8 for both models. More specifically, the younger craters are spectrally bluer, which is consistent with the results found by [Stephan et al. \(2019\)](#), who used a ratio between two filters, $0.437 \mu\text{m}$ and $0.749 \mu\text{m}$, of the Dawn Framing Camera. Assuming that the region outside the craters is the oldest, the youngest craters have a bluer slope beyond 1σ boundaries. This suggests a relation between the age and color on Ceres, possibly related to the space weathering effect. It is an optically nonlinear effect dependent on the exposure time according to the results obtained from laboratory experiments ([Brunetto et al. 2006](#); [Lantz et al. 2017](#)). We found a similar relation in Ceres' craters. This behavior fits the following function for each dating model:

$$S_{\text{VIS}}(t_{\text{ADM}}) = (3.6 \pm 0.6 \times \ln(t_{\text{ADM}}) + 4 \pm 3) \times 10^{-6} \quad | \quad R^2 = 0.7 ,$$

$$S_{\text{VIS}}(t_{\text{LDM}}) = (3.0 \pm 0.4 \times \ln(t_{\text{LDM}}) + 5 \pm 2) \times 10^{-6} \quad | \quad R^2 = 0.7 .$$

[Stephan et al. \(2019\)](#) also note that invoking space weathering is mandatory for explaining this behavior. However, the composition, grain size ([Sultana et al. 2021](#)), porosity ([Poch et al. 2016](#); [Schröder et al. 2021](#)), and mixing modalities ([Rousseau et al. 2018](#)) also affect spectral slopes. Caution must therefore be exercised when interpreting these results. In the VNIR and VNUV ranges, although the fit also follows a reddening trend with age, every slope value of the craters is compatible with the 1σ limit defined by the region outside the craters, thus, no further conclusions could therefore be reached.

It is known that large impacts have a low probability of forming ([Marchi et al. 2012, 2016](#)), so it is expected that the larger the crater, the older it is. If the spectral slope is a proxy of the crater age, the probability of there being large craters as blue as younger craters should be low. Following this line of reasoning, we see in the right panel of [Fig. 7](#) how craters with a

diameter greater than 100 km are found mainly in the red part of the distribution with a median visible slope of $(2.5 \pm 0.6) \times 10^{-5} \text{ \AA}^{-1}$. This range of slopes is in good agreement with that of the surface outside craters. Meanwhile, craters smaller than 100 km are quite spread over the color space with a bluer median visible slope of $(1.6 \pm 1.0) \times 10^{-5} \text{ \AA}^{-1}$.

As we have mentioned in [Section 1](#), our target asteroids are in the pristine region, have mainly been preserved since their formation, and would probably have originated through impacts that produced craters with diameters of several hundreds of kilometers ([Carruba et al. 2016](#)). These lines of evidence imply that the asteroids belonging to the Ceres collisional family should belong to the redder part of this overpopulation, where the largest and oldest craters are located, assuming the craters and asteroid family optically evolve in the same manner according to age. Thus, the blueness of 61674 suggests that it is less likely to be a member of a collisional family of Ceres. On the other hand, 6671 has redder slopes compatible with more weathered material. However, the presence of an absorption band, only reported in the surroundings of the young Occator crater ($17.8 \pm 1.2 \text{ Ma}$) on the surface of Ceres, suggests that it is as fresh as this crater. Nevertheless, members of asteroid families could collide and generate a second, fresher generation of asteroids ([Marchi et al. 2006](#)). The collisional timescale depends on the diameter of the family members; 6671 and 61674 have a diameter of 13.75 and 8.21 km, respectively ([Carruba et al. 2016](#)). According to [Bottke et al. \(2005\)](#), the average collisional lifetime of 10 km diameter asteroids is 4.7 Ga. Following the new models for collisional disruptions in [Bottke et al. \(2020\)](#), we obtained a collisional lifetime of $\sim 6 \text{ Ga}$. The mean age of main belt asteroids (T_{MB}) depends on the collisional lifetime (τ_{coll}) and the late heavy bombardment age (t_{LHB}) following the formula given by [Marchi et al. \(2006\)](#):

$$T_{\text{MB}} \approx \tau_{\text{coll}} \left[1 - \left(1 + \frac{t_{\text{LHB}}}{\tau_{\text{coll}}} \right) e^{-t_{\text{LHB}}/\tau_{\text{coll}}} \right] + t_{\text{LHB}} e^{-t_{\text{LHB}}/\tau_{\text{coll}}} .$$

Using $\tau_{\text{coll}} \in (4.7, 6) \text{ Ga}$ and $t_{\text{LHB}} \in (4, 4.5) \text{ Ga}$, we obtain $T_{\text{MB}} \in (2.7, 3.2) \text{ Ga}$, which is older than the highest age estimate for craters on the surface of Ceres (1.6 Ga) but of the same order of magnitude. Even though this line of argument indicates that those two asteroids are less likely to be part of the collisional family, one has to consider that collisional models also suggest that larger impacts may have happened in the past ([Marchi et al. 2016](#)), having been hidden by a resurfacing process.

6. Conclusions

Here, we have presented a spectroscopic study at visible wavelengths of 14 asteroids selected from the list of potential members of a collisional family of Ceres by [Carruba et al. \(2016\)](#). We have reached the following conclusions:

- After taxonomic classification of the asteroids, comparison of their spectral slopes with that of Ceres itself, and with the distribution of slopes across the latter's surface, 12 out of the 14 asteroids are found not to be compatible with Ceres' spectra.
- In one of the other two asteroids, 6671, we have detected an absorption band at $0.7 \mu\text{m}$, which indicates the presence of hydrated silicates. Although there is strong evidence of hydration in Ceres, this $0.7 \mu\text{m}$ band has not been detected in any of the Dawn/VIR spectra or in the ground-based spectra

Name	D (km)	Latitude (deg)	Longitude (deg)	LDM (Ma)	ADM (Ma)
Achita	40	25.82	65.96	570 ± 60	160 ± 20
Azacca	49.9	-6.66	218.4	75.9 ± 10	45.8 ± 5
Cacaguat	13.6	-1.2	143.6	1.3 ± 0.79	1.55 ± 0.8
Centeotl	6.0	18.9	141.2	4.2 ± 3	6.7 ± 4
Coniraya	135	39.9	65.7	1300 ± 300	1100 ± 500
Dantu	126	24.3	138.2	111 ± 39	-
Ernutet	53.4	52.9	45.5	1600 ± 200	420 ± 60
Gaue	80	30.8	86.2	260 ± 30	76 ± 6
Haulani	34	5.8	10.8	2.7 ± 0.7	3.4 ± 0.5
Ikapati	50	33.8	45.6	19.2 ± 2.2	19.4 ± 1.9
Kerwan	280	-10.8	124	1300 ± 160	281 ± 17
Liber	23	42.6	37.8	440 ± 60	180 ± 20
Messor	40	49.9	233.7	64.5 ± 2.6	46.8 ± 4.9
Occator	92	19.8	239.3	17.8 ± 1.2	-
Omonga	77	58.0	71.7	970 ± 70	250 ± 20
Oxo	10	42.2	359.6	0.5 ± 0.2	0.5 ± 0.2
Rao	12	8.1	119.0	33.1 ± 2.5	33.6 ± 2.5
Sintana	58	-48.1	46.2	310 ± 40	120 ± 10
Tupo	36	-32.3	88.4	49 ± 8	32 ± 3
Urvara	170	-46.6	249.2	134 ± 8	-
Yalode	260	-42.6	292.5	1100 ± 450	-
Unnamed	34	39	247	906 ± 130	242 ± 24
Unnamed	15	23	186	205 ± 12	88.1 ± 17
Unnamed	34	-43.3	120.9	1330 ± 270	272 ± 41
AhunaMons	20	-10.3	316.5	70 ± 20	70 ± 20

Table 3. Summary table with name, diameter, location, and estimated age for every crater from [Stephan et al. \(2019\)](#) used in this study.

of Ceres. The only detection so far is the one by [Rizos et al. \(2019\)](#) in the surroundings of the young Occator crater using photometric data from the Dawn Framing Camera. The band depth measured for 6671 is in agreement with that from [Rizos et al. \(2019\)](#), but it is also in good agreement with the values typically observed in other primitive asteroids throughout the main belt ([Morate et al. 2016, 2018](#)).

- Our results strongly suggest that material on the surface of Ceres gets redder with time in the visible wavelength range. The blueness of the other compatible asteroid, 61674, makes it compatible with fresher crater material.
- We expect that asteroids with diameters of tens of kilometers that belong to a Ceres collisional family located in the pristine region are probably as red as the oldest craters. The compatibility of both 6671 and 61674 with fresh Ceres material suggest that they are not likely to be members of such a collisional family. As we should also consider the possibility that they are refreshed second generation objects, we cannot refute that this family exists or has existed. More potential members need to be observed in order to confirm or reject the existence of such a family.

Acknowledgements. FTR, JdL, ET, and JLR acknowledge financial support from the project PID2020-120464GB-I100 of the Spanish Ministerio de Ciencia e Innovación (MICINN).

Based on observations made with the Gran Telescopio Canarias (GTC), under observational program GTC68-17A. We especially thank David Morate for sharing his time.

References

Bottke, W. F., Durda, D. D., Nesvorný, D., et al. 2005, *Icarus*, 179, 63
 Bottke, W. F., Vokrouhlický, D., Ballouz, R. L., et al. 2020, *AJ*, 160, 14
 Brunetto, R., Romano, F., Blanco, A., et al. 2006, *Icarus*, 180, 546

Bus, S. J. & Binzel, R. P. 2002a, *Icarus*, 158, 146
 Bus, S. J. & Binzel, R. P. 2002b, *Icarus*, 158, 106
 Carrozzo, F. G., Raponi, A., De Sanctis, M. C., et al. 2016, *Review of Scientific Instruments*, 87, 124501
 Carruba, V., Nesvorný, D., Marchi, S., & Aljbaae, S. 2016, *Monthly Notices of the Royal Astronomical Society*, 458, 1117
 Cellino, A., Bus, S. J., Doressoundiram, A., & Lazzaro, D. 2002, *Spectroscopic Properties of Asteroid Families* (University of Arizona Press, Tucson), 633–643
 Cepa, J. 2010, *Astrophysics and Space Science Proceedings*, 14, 15
 Cepa, J., Aguiar, M., Escalera, V. G., et al. 2000, in *Society of Photo-Optical Instrumentation Engineers (SPIE) Conference Series*, Vol. 4008, *Optical and IR Telescope Instrumentation and Detectors*, ed. M. Iye & A. F. Moorwood, 623–631
 Chapman, C. R. & Gaffey, M. J. 1979, *Spectral reflectances of the asteroids*, ed. T. Gehrels & M. S. Matthews, 1064–1089
 Ciarniello, M., Capaccioni, F., Filacchione, G., et al. 2015, *A&A*, 583, A31
 Ciarniello, M., De Sanctis, M. C., Ammannito, E., et al. 2017, *Astronomy & Astrophysics*, 598, A130
 de Sanctis, M. C., Ammannito, E., Raponi, A., et al. 2015, *Nature*, 528, 241
 de Sanctis, M. C., Coradini, A., Ammannito, E., et al. 2011, *Space Sci. Rev.*, 163, 329
 DeMeo, F. E., Binzel, R. P., Slivan, S. M., & Bus, S. J. 2009, *Icarus*, 202, 160
 Fornasier, S., Lantz, C., Barucci, M. A., & Lazzarin, M. 2014, *Icarus*, 233, 163
 Fornasier, S., Lazzarin, M., Barbieri, C., & Barucci, M. A. 1999, *Astronomy & Astrophysics Supplement*, 135, 65
 Fujiya, W., Hoppe, P., Ushikubo, T., et al. 2019, *Nature Astronomy*, 3, 910
 Hiesinger, H., Marchi, S., Schmedemann, N., et al. 2016, *Science*, 353, aaf4758
 Knezevic, Z., Lemaître, A., & Milani, A. 2002, in *Asteroids III*, ed. W. F. J. Bottke, A. Cellino, P. Paolicchi, & R. P. Binzel (University of Arizona Press, Tucson), 603–612
 Lantz, C., Brunetto, R., Barucci, M. A., et al. 2017, *Icarus*, 285, 43
 Lazzaro, D., Angeli, C. A., Carvano, J. M., et al. 2004, *Icarus*, 172, 179
 Lebofsky, L. A., Feierberg, M. A., Tokunaga, A. T., Larson, H. P., & Johnson, J. R. 1981, *Icarus*, 48, 453
 Marchi, S., Ermakov, A. I., Raymond, C. A., et al. 2016, *Nature Communications*, 7, 12257
 Marchi, S., McSween, H. Y., O'Brien, D. P., et al. 2012, *Science*, 336, 690
 Marchi, S., Paolicchi, P., Lazzarin, M., & Magrin, S. 2006, *AJ*, 131, 1138
 McFadden, L. A., Gaffey, M. J., & McCord, T. B. 1984, *Icarus*, 59, 25
 Milani, A., Cellino, A., Knezevic, Z., et al. 2014, *Icarus*, 239, 46

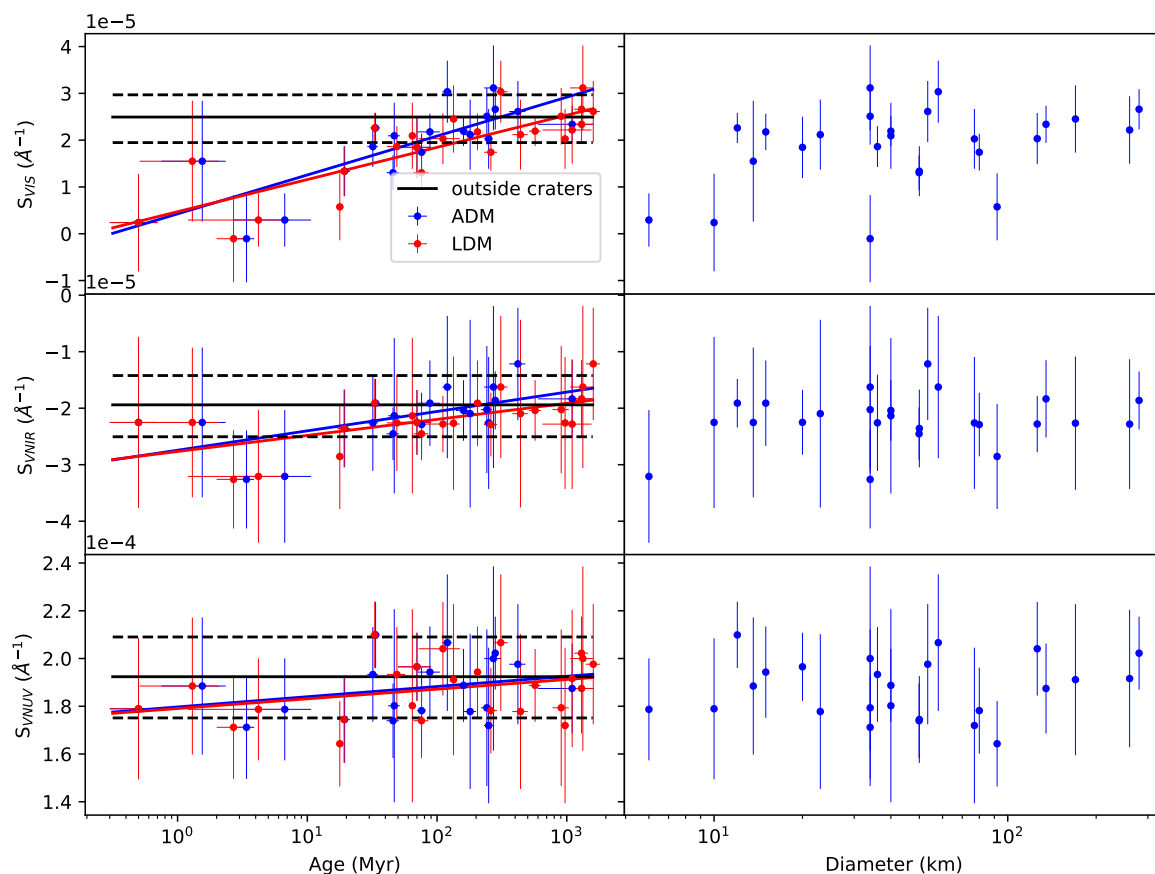


Fig. 7. Relation between the median spectral slopes in the three different wavelength ranges described in Section 3 for craters on the surface of Ceres with their age (left) and size (right). The upper panel corresponds to S_{VIS} , the central panel to S_{VNIR} , and the lower panel to S_{VNUV} . The represented ages are from two models: the asteroid derived model (in blue) and the lunar derived model (in red). The median slope value of the region outside the craters is represented with a horizontal black line. The dashed lines mark the 16th and 85th percentiles. Solid lines correspond to the least squares fit for each model.

- Morate, D., de León, J., De Prá, M., et al. 2018, *Astronomy & Astrophysics*, 610, A25
Morate, D., de León, J., De Prá, M., et al. 2016, *Astronomy & Astrophysics*, 586, A129
Nathues, A., Hoffmann, M., Platz, T., et al. 2016, *Planet. Space Sci.*, 134, 122
Neesemann, A., van Gasselt, S., Schmedemann, N., et al. 2019, *Icarus*, 320, 60
Nesvorný, D., Brož, M., & Carruba, V. 2015, *Identification and Dynamical Properties of Asteroid Families*, 297–321
Perna, D., Kaňuchová, Z., Ieva, S., et al. 2015, *A&A*, 575, L1
Poch, O., Pommerol, A., Jost, B., et al. 2016, *Icarus*, 267, 154
Popescu, M., Birlan, M., & Nedelcu, D. A. 2012, *Astronomy & Astrophysics*, 544, A130
Reddy, V., Li, J.-Y., Gary, B. L., et al. 2015, *Icarus*, 260, 332
Rivkin, A. S. 2012, *Icarus*, 221, 744
Rivkin, A. S., Volquardsen, E. L., & Clark, B. E. 2006, *Icarus*, 185, 563
Rizos, J. L., de León, J., Licandro, J., et al. 2019, *Icarus*, 328, 69
Rousseau, B., De Sanctis, M. C., Raponi, A., et al. 2020, *A&A*, 642, A74
Rousseau, B., Éard, S., Beck, P., et al. 2018, *Icarus*, 306, 306
Schröder, S. E., Poch, O., Ferrari, M., et al. 2021, *Nature Communications*, 12
Stephan, K., Jaumann, R., Zambon, F., et al. 2019, *Icarus*, 318, 56
Sultana, R., Poch, O., Beck, P., Schmitt, B., & Quirico, E. 2021, *Icarus*, 357, 114141
Usui, F., Hasegawa, S., Ootsubo, T., & Onaka, T. 2019, *PASJ*, 71, 1
Valsecchi, G. B., Carusi, A., Knezevic, Z., Kresak, L., & Williams, J. G. 1989, in *Asteroids II*, ed. R. P. Binzel, T. Gehrels, & M. S. Matthews, 368–385
Vernazza, P., Mothé-Diniz, T., Barucci, M. A., et al. 2005, *A&A*, 436, 1113
Vilas, F. 1994, *Icarus*, 111, 456
Vilas, F. & Gaffey, M. J. 1989, *Science*, 246, 790
Vilas, F., Larson, S. M., Hatch, E. C., & Jarvis, K. S. 1993, *Icarus*, 105, 67
Vilas, F. & McFadden, L. A. 1992, *Icarus*, 100, 85
Zellner, B., Tholen, D. J., & Tedesco, E. F. 1985, *Icarus*, 61, 355